Available online at www.sciencedirect.com
ScienceDirect
Journal of the European Ceramic Society 31 (2011) 745–753
www.elsevier.com/locate/jeurceramsoc

Strength reliability of 3D low temperature co-fired multilayer ceramics under biaxial loading

R. Bermejo [a,*], P. Supancic [a,b], I. Kraleva [b], R. Morrell [c], R. Danzer [a,b]

[a] *Institut für Struktur- und Funktionskeramik (ISFK), Montanuniversität Leoben, A-8700 Leoben, Austria*
[b] *Materials Center Leoben Forschung GmbH (MCL), A-8700 Leoben, Austria*
[c] *National Physical Laboratory (NPL), Teddington, Middlesex TW11 0LW, UK*

Received 6 July 2010; received in revised form 16 November 2010; accepted 28 November 2010
Available online 21 December 2010

Abstract

Low temperature co-fired ceramics (LTCCs) are multilayered ceramic based components, which can be used as high precision electronic devices in highly loaded environments. In many applications, LTCC end components are exposed to mechanical stresses, which may yield different types of failure coming from different locations, thus decreasing the mechanical reliability of the device. The aim of this work is to assess the mechanical strength of LTCC parts and investigate the influence of the metal internal structure (supporting the maximum load) on the local fracture response. Strength of different positions (e.g. near vias, metal-pads, ceramic layers) has been measured under biaxial loading and compared with a reference bulk LTCC. The strength results were interpreted in the framework of Weibull theory. Fractographic analyses revealed a significant effect of the first metallisation layer below the tensile surface on the strength reliability of the structure, which should be considered to optimise LTCC designs.

Keywords: LTCC; Glass ceramics; Strength; Fracture; Functional applications

1. Introduction

Low temperature co-fired ceramics (LTCCs) are layered ceramic based components, which can be used as electronic devices (e.g. for mobile and automotive technologies) in highly loaded (temperatures, inertia forces, etc.) environments. They consist of a complex three-dimensional micro-network of metal structures embedded within a glass-containing ceramic substrate. LTCC technology was established in the 1970s as an alternative to overcome conductivity problems with tungsten metallisation in alumina substrates employed in high temperature co-fired ceramics.[1] Co-firing is an attractive approach for producing these structural laminates. The low sintering temperature in LTCCs (*i.e.* below 950 °C) can be achieved by using a glass matrix with a low softening point, allowing a liquid phase sintering of the ceramic composite material.[2] This makes feasible the use of excellent conductors such as silver, gold or mixtures of silver–palladium, arranged within and/or on the surfaces of the ceramic substrate, forming complex multi-layered structures. Today, they can be found in devices which have to operate under harsh conditions such as high temperatures and mechanical shock. These applications include engine control units, automatic gear box control units, ABS, etc. For instance, the electronics for engine and gear management are installed close to the engine and gears, where temperatures up to 150 °C and vibration loads of high accelerations (e.g. up to 100 g) can be encountered in extreme cases. As the usage of electronic systems increases over time by the *x*-by-wire technology (e.g. brake-by-wire, steer-by-wire), and because such applications have strong safety implications, it is mandatory to assess the reliability of the ceramic substrates.

The brittle nature of ceramic based materials such as LTCC creates challenges for selecting both a material and a design to meet the performance of a particular system. The outcome of competition between various classes of materials is given not only by the combination of their intrinsic properties but also by the processing capability that they may offer for being tailored for specific tasks. In addition, the flaw distribution (size,

* Corresponding author.
E-mail addresses: raul.bermejo@unileoben.ac.at, raul.bermejo@mu-leoben.t (R. Bermejo), phs@unileoben.ac.at (P. Supancic), irina.kraleva@mcl.at (I. Kraleva), roger.morrell@npl.co.uk (R. Morrell), robert.danzer@unileoben.ac.at (R. Danzer).

0955-2219/$ – see front matter © 2010 Elsevier Ltd. All rights reserved.
doi:10.1016/j.jeurceramsoc.2010.11.031

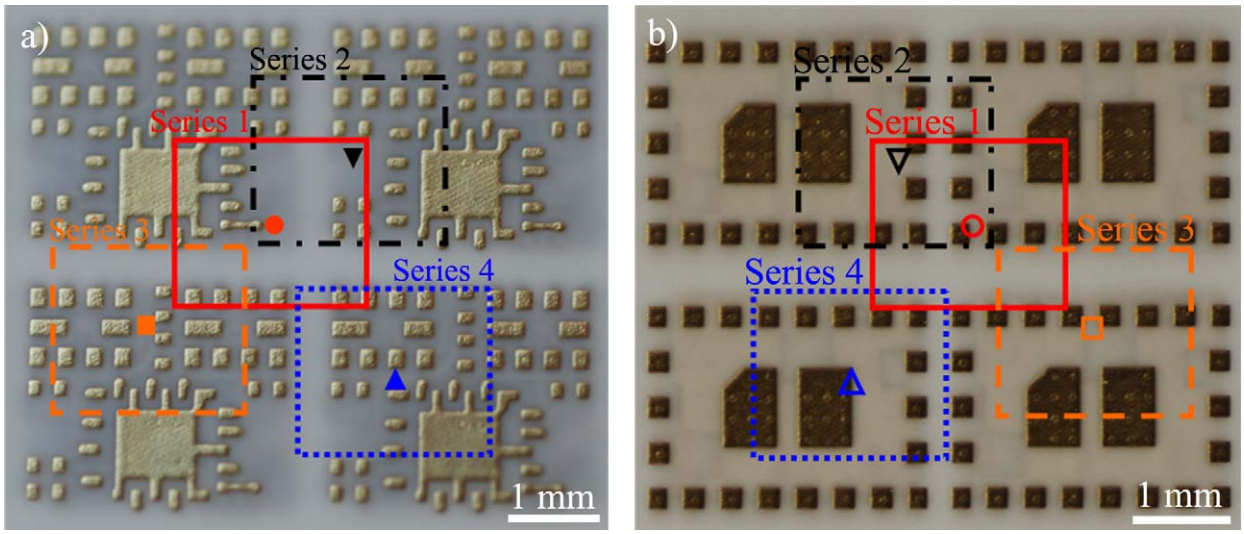

Fig. 1. Scheme of a panel where the samples are cut out in such a way that the position to be tested lies in the centre of the specimen: a) with the upper side and b) with the lower side under tension.

location, etc.) and size effect in ceramic containing materials yield a statistical strength distribution (described by the Weibull theory[3]) which conditions the mechanical reliability of ceramic components.[4–6] The development and implementation of multilayered structures (e.g. metal–ceramic, ceramic–ceramic) for structural and/or functional applications in the recent past is an excellent example of the design and material selection approaches mentioned above.

As a matter of fact, the brittle fracture of monolithic ceramic materials has been overcome by introducing layered architectures of different kinds, *i.e.* geometry, composition of layers, residual stresses, interface toughness, etc. The main goal of such layered designs has been to enhance the fracture energy of the system on one hand and to increase the strength reliability of the end component on the other hand (see for instance Refs. [7–13]). Although LTCC-based components are more complex material systems than laminates with continuous layers, many features involved in the co-firing process are similar. For instance, in the co-firing of layered structures, residual stresses may arise as a result of differences in the shrinkage behaviour between adjacent layers, which can also be the case between LTCC layers and metal structures.[14] Also the disposition of the metal electrodes within the LTCC part may have an effect on the mechanical behaviour of the component. In this regard, the effect of metallisation on the strength distribution has been assessed in the literature using simple architectures yielding a difference not only on the strength values but also on the critical flaw size distribution (Weibull modulus) associated with the presence of vias in the design.[15]

In general, the biaxial strength of ceramics can be determined by several methods, as found in Ref. [16]. In particular, strength of planar LTCC components has been determined using the ball-on-ring (BOR) test[17] or the ring-on-ring (ROR) test[18] on bulk specimens. These methods induce a maximal biaxial stress distribution in the centre of the specimen and avoid the influence of edge effects. However, it has been shown that, during these tests, small geometric inaccuracies (e.g. for the case of "as-sintered" specimens) could lead to an undefined load transfer from the rings to the specimen and thus cause large uncertainties in the determined strength.[19] This is specially enhanced when testing small specimens. In this regard, such uncertainties can be minimised when a different loading configuration, the ball-on-three-balls (B3B) test, is used.[20–23] Despite the small effective volume tested with this method, localised strength measurements (*i.e.* near metal contacts, vias, etc.) can be performed even in miniaturised (e.g. less than 0.5 mm^3) components. Thus, the influence of micro-sized surface features on strength can be assessed to determine the reliability of the embedded component.

In this work, the effect of metallisation on the strength of LTCCs as function of the location within the part has been investigated using the B3B test. The mechanical behaviour of LTCC components during biaxial bending has been analysed in special positions of the part. The strength has been evaluated using Weibull statistics and a fractographic analysis of broken specimens has been performed to determine the mode of fracture of the components and the influence of the internal architecture (*i.e.* metal-electrodes, pads, ceramic layers) on the LTCC strength reliability.

2. Experimental procedure

2.1. Material of study

The specimens used for the biaxial strength tests were cut from commercial MKE100 LTCC-Tapes (panels of ca. 100 mm × 100 mm × 0.43 mm), provided by the company EPCOS OHG, Deutschlandsberg, Austria. The substrate (glass–ceramic) is made of approx. 50% of Al_2O_3 as filler and 50% of several glasses containing Ca, Na, Si, K, B and Al, where the crystallisation degree after sintering exceeds 90%. For the inner metallisation only Ag is used, whereas for the outer metallisation the silver pads are covered with a nanometric Ni/Au layer, which is employed to about corrosion and

further guarantees good adhesion of possible soldered components. The thickness of the metal pads is approx. 7 μm. The processing route employed was tape casting and the co-sintering was performed in a furnace at 850 °C. After sintering, rectangular testing plates of ca. 11.0 mm × 9.7 mm × 0.43 mm were cut from each panel (see detail in Fig. 1). The dicing of the LTCC specimens was performed with a diamond saw. The parts were cut in such a way that different locations of the LTCC could be placed in the potential region of maximal tensile stress during testing, thus well defined strengths within the part could be evaluated. Four series of at least 30 LTCC specimens were selected for the strength measurements of both the upper (Fig. 1a) and lower (Fig. 1b) side of the components (*i.e.* series 1–4). Each series has the same internal ceramic–metal layered architecture. The difference between them lies on the particular feature to be tested located at the region of maximal stress (e.g. metal pad, glass–ceramic, metal via) during biaxial loading and the internal architecture underneath. An additional series of 30 bulk specimens (without metallisation) produced with the same processing route was also tested for comparison. A total of ca. 300 specimens were tested for this study.

2.2. Mechanical testing: B3B method

The mechanical strength of commercial LTCC plate-like components during biaxial bending was investigated using the B3B test, analysing four special positions (series) both at the upper and lower side of the component. In the B3B method, a rectangular plate (or a disc) is symmetrically supported by three balls at one plane and loaded by a fourth ball in the centre of the opposite plane (Fig. 2a). Details about the test can be found elsewhere.[24] In our case all four balls had a diameter of 8 mm. A pre-load of 7 N was applied to hold the specimen between the four balls. Then, the tests were conducted under displacement control at a rate of 0.5 mm/min and a relative humidity (RH) of 23 ± 2% at 21 ± 1 °C (*i.e.* $H_{abs} \approx 4.3 \pm 0.4\ g_{H_2O}/m^3$), using a universal testing machine (Zwick Z010, Zwick/Roell, Ulm, Germany) with a load cell of 200 N. The load was increased until fracture occurred and the fracture load was used to calculate the maximum tensile biaxial stress in the specimen at the moment of fracture.

2.3. Assessment of biaxial strength

For a bulk plate of an elastically isotropic material the maximum stress σ_{max} corresponding to the fracture load, P, can be calculated as follows:

$$\sigma_{max} = f \cdot \frac{P}{t^2} \tag{1}$$

where t is the plate thickness and f is a dimensionless factor, which depends on the geometry of the specimen and the balls, Poisson's ratio of the tested material and details of the load transfer from the jig into the specimen,[24] *i.e.* positioning of the loading ball (symmetric or asymmetric), etc. In order to determine such factor f, a FEM linear elastic analysis was performed using the software ANSYS 11.0 for the testing geometry.[25] Elastic properties were determined by means of the Resonant Beam Method[26] in a bulk LTCC sample, resulting in a Young's modulus of $E = 113 \pm 1$ GPa and a Poisson's ratio of $\nu = 0.2 \pm 0.01$. Thus, the factor f was calculated for the given geometry and Poisson's ratio as function of the thickness of the specimens, and linearly fitted giving as a result[27]:

$$f = 2.58 - 0.67 \cdot \left(\frac{t}{t_0} - 1\right)$$
$$(\text{valid for } 0.40 < t < 0.46\ \text{mm and } n = 0.2) \tag{2}$$

The parameter $t_0 = 0.43$ mm is defined as the mean thickness of the plates. The corresponding stress distribution in the plate during biaxial loading is shown in Fig. 2b. The maximal stress is located in the centre of the three balls. It can be inferred from the referred figure that the central region, *i.e.* approx. 1/20 of the specimen dimension, is stressed with more than 90% of the maximal stress. Therefore, localised strength measurements can be performed. For instance, a detail of the stress distribution in a specimen from series 2 with the upper side under tension can be seen in Fig. 3. A crack running through the region of maximal stress can be also appreciated.

The accuracy of this method in determining the maximal stress has been compared with other methods such as the ball-on-ring-test. The accuracy of the analytical solution for the latter depends on the selection of the equivalent radius of contact associated with the contact load.[16] If we compared the stresses

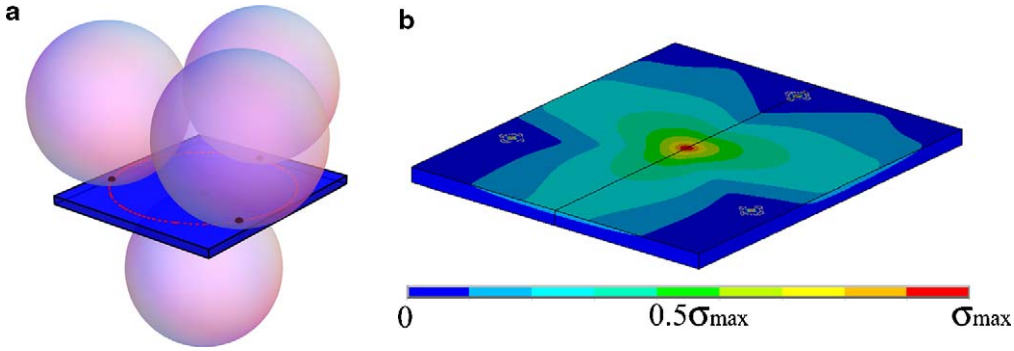

Fig. 2. a) Scheme of the ball-on-three-balls test for biaxial testing and b) FE simulation of the stress distribution in the plate during loading. The central region in contains stresses greater than 90% of the maximum stress in the plate.

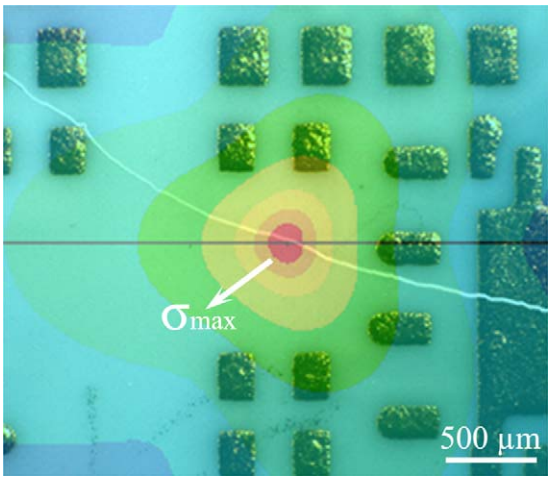

Fig. 3. Tensile stress distribution superimposed on the tensile surface of a tested LTCC specimen (corresponding to series 2 with the upper part under tension); a crack running through the location of maximal stress can be appreciated (see arrow).

resulting with the analytical formulation for the same geometry with (i) the B3B on a disc[24] and (ii) the B3B on the plate of study (with equal section as the disc), the analytical method underestimates the stresses in ≈5% compared to (i) and ≈10% compared to (ii). Nevertheless, the analytical solution can be used for ranking materials. But if an accurate solution is pursued the B3B approach is recommended.

We caution the reader that Eq. (1) estimates the failure stress in the B3B test for isotropic (bulk) materials, with respect to thickness in a given range. Since the thickness is claimed to be the most crucial parameter in the evaluation of the failure stress,[21] it has been measured in the centre of all samples before testing. Furthermore, the influence of the metallic structures on the stress distribution has been neglected due to the small contribution of the elastic modulus of the metals to the whole compliance of the part (*i.e.* approx. $E = 85$ GPa). This assumption has been checked by comparing the compliance of bulk specimens under bending and specimens containing metallisation. In addition, the effect of the surface metal features on the thickness of the specimens for the stress calculation with Eq. (1) has been also neglected. As a result, the total thickness measured in the centre of the specimens has been considered as the effective thickness (t) for the calculation of an "equivalent" maximum stresses with Eq. (1) for a homogeneous plate-like specimen.

The strength results were analysed in the framework of the Weibull theory. A fractographic investigation was performed using an optical stereo microscope (Olympus SZH10, Austria) for every series to identify the mode of failure and the influence of the internal layered architecture on the crack propagation through the LTCC part.[28,29] The load–displacement curves of the B3B tests were also examined for a better understanding of the fracture process.

3. Results and discussion

3.1. Load–displacement curves

Some characteristic load–displacement curves of all series (1–4) for specimens with the upper side as well as with the lower side under tension are presented in Fig. 4a and b, respectively. A bulk specimen is also shown for comparison.

The brittle behaviour of the bulk specimens is associated with the linear behaviour to fracture seen in the load–displacement curves. On the other hand, some of the series with metal structures present step-like fracture behaviour, *i.e.* the initial propagation of the critical defect during loading does not yield catastrophic failure. Instead, the material can withstand further displacement before complete fracture. The effect of metallisation may affect the strength distribution of the material and shall be discussed below.

3.2. Weibull analysis of strength results

Figs. 5 and 6 show a Weibull diagram of the four LTCC series, tested either with the upper side or with the lower side under tension, respectively. Each distribution was collected on a sample of 30 specimens, which ensures statistical significance for the Weibull analysis. The nominal failure load, P_f, is represented vs. the probability of failure (Figs. 5a and 6a). P_f has been defined as the load corresponding to the first kink in the load–displacement curves (see Fig. 4), based on the consideration that after the first rupture of the glass–ceramic layer the functionality of the LTCC component may be damaged. The corresponding equivalent fail-

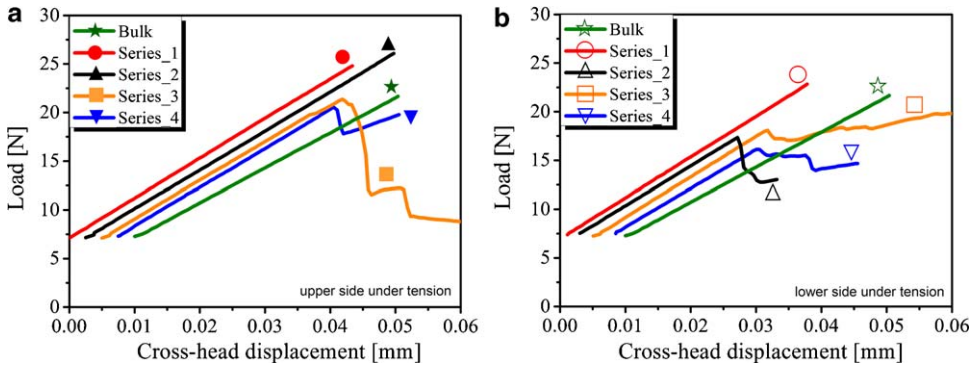

Fig. 4. Load vs. displacement curves and fracture features of characteristic specimens of the tested series with (a) upper and (b) lower side under tension.

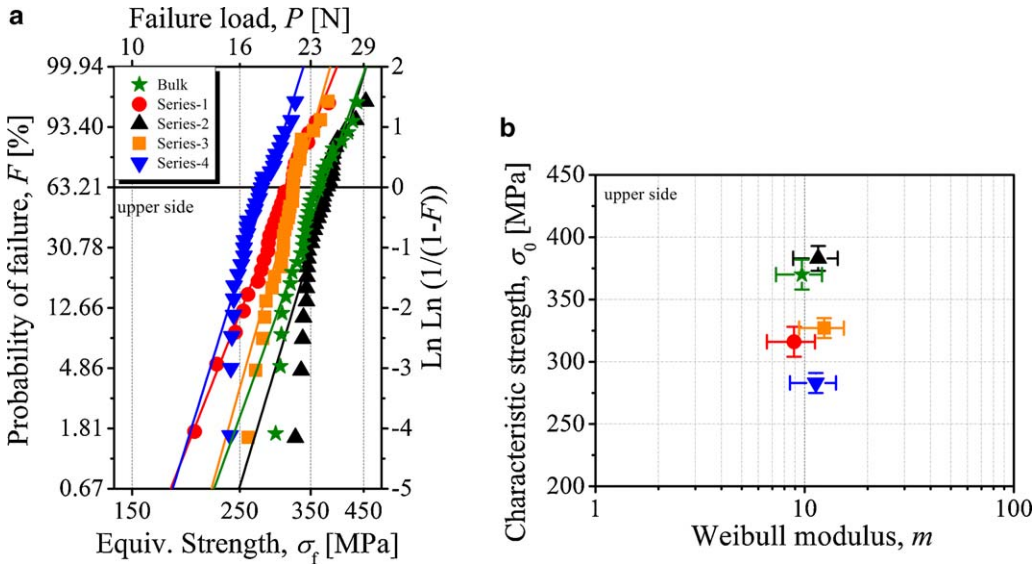

Fig. 5. a) Weibull diagram of four LTCC series (upper side under tension) and bulk material; b) the characteristic strength, σ_0, is also plotted vs. the Weibull modulus, m.

ure stress, σ_f, calculated with Eq. (1) for every tested specimen is also presented in the plot. The strength results from the bulk specimens are also represented for comparison.

The characteristic failure load P_0 (*i.e.* the load with a probability of failure of $F = 63.21\%$) for all four locations is also plotted vs. the Weibull modulus, m (biased), in Fig. 5a and b. The strength results of the bulk specimens are also represented for comparison. The characteristic equivalent strength values and Weibull moduli of all series as well as the corresponding 90% confidence intervals can be found in Table 1.

The effective volume for all series has been evaluated from the FE analysis following the principle of independent actions (PIA)[30] and taking into account the corresponding m, resulting in $V_{eff} \approx 2 \times 10^{-3}\,mm^3$.

It can be inferred from Figs. 5a and 6a that all series follow a Weibull distribution. Nevertheless, the strength distribution between some of the series with metallisation and the bulk series is different, both for the upper side (Fig. 5a) and the lower side (Fig. 3b) under tension. Some of the diagrams seem to follow a typical two-parameter Weibull distribution (e.g. series 1 in Fig. 6a), whereas others show a so-called "*concave banana-shape*" (*i.e.* the strength distribution in the Weibull diagram deviates from a lineal trend, pointing downwards for lower failure stress values). In such cases (see for instance series 2 and 4 in Fig. 5a) a unique minimum failure stress level ("*threshold stress*") can be defined under which the material would not fail. This would enhance the mechanical reliability of LTCC components, similar to the

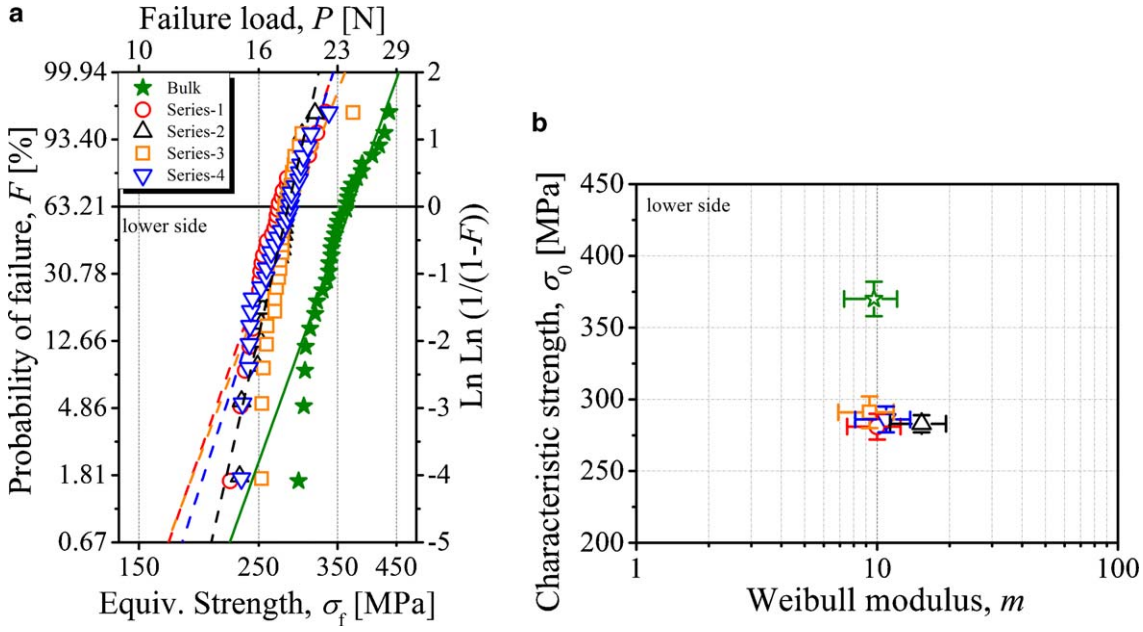

Fig. 6. a) Weibull diagram of four LTCC series (lower side under tension) and bulk; b) the characteristic strength, σ_0, is also plotted vs. the Weibull modulus, m.

Table 1
Characteristic strength values, σ_0, and Weibull moduli, m, for all series with the corresponding 90% confidence intervals.

Series	Characteristic strength, σ_0 [MPa] (90% confidence interval)		Weibull modulus, m (90% confidence interval)	
	Upper side under tension	Lower side under tension	Upper side under tension	Lower side under tension
Series 1	316 (304–329)	281 (272–291)	8.9 (6.6–10.9)	10.0 (7.5–12.0)
Series 2	383 (373–394)	284 (277–290)	11.6 (8.8–14.1)	15.3 (11.3–18.7)
Series 3	327 (319–336)	291 (280–302)	12.4 (9.4–15.1)	9.3 (6.9–11.3)
Series 4	283 (275–291)	286 (277–295)	11.3 (8.5–13.7)	10.9 (8.1–13.3)
Bulk	370 (358–383)		9.7 (7.3–11.8)	

case reported on other layered ceramic architectures (see for instance[31–33]).

In addition a statistically significant difference in the equivalent characteristic strength of the components is found between the upper side and the lower side loaded under tension, *i.e.* $\sigma_0 = 283–383$ MPa and $\sigma_0 = 281–294$ MPa, respectively (Figs. 5b and 6b). A rather constant strength value, σ_0, for the latter, regardless of the location tested should be highlighted, which is significantly smaller than σ_0 of the bulk series, *i.e.* $\sigma_0 = 370$ MPa.

Regarding the Weibull moduli, no statistically difference could be found between both orientations (upper side or lower side under tension), being $m = 8.9–12.4$ and $m = 9.3–15.3$ respectively, being similar to the Weibull modulus obtained for the bulk specimens ($m = 9.7$). This suggests similar flaw populations for LTCCs with metallisation and for bulk LTCCs.

Based on a linear elastic fracture mechanics (LEFM) approach, the critical defect size (a_c) causing the failure of the biaxial loaded specimens can be estimated based on the failure stress (defined as equivalent stress as in Figs. 5a and 6a), σ_f, and on the fracture toughness, K_{Ic}, of the material as given by the following equation[34,35]:

$$a_c = \frac{1}{\pi} \cdot \left(\frac{K_{Ic}}{Y\sigma_f} \right)^2, \quad (3)$$

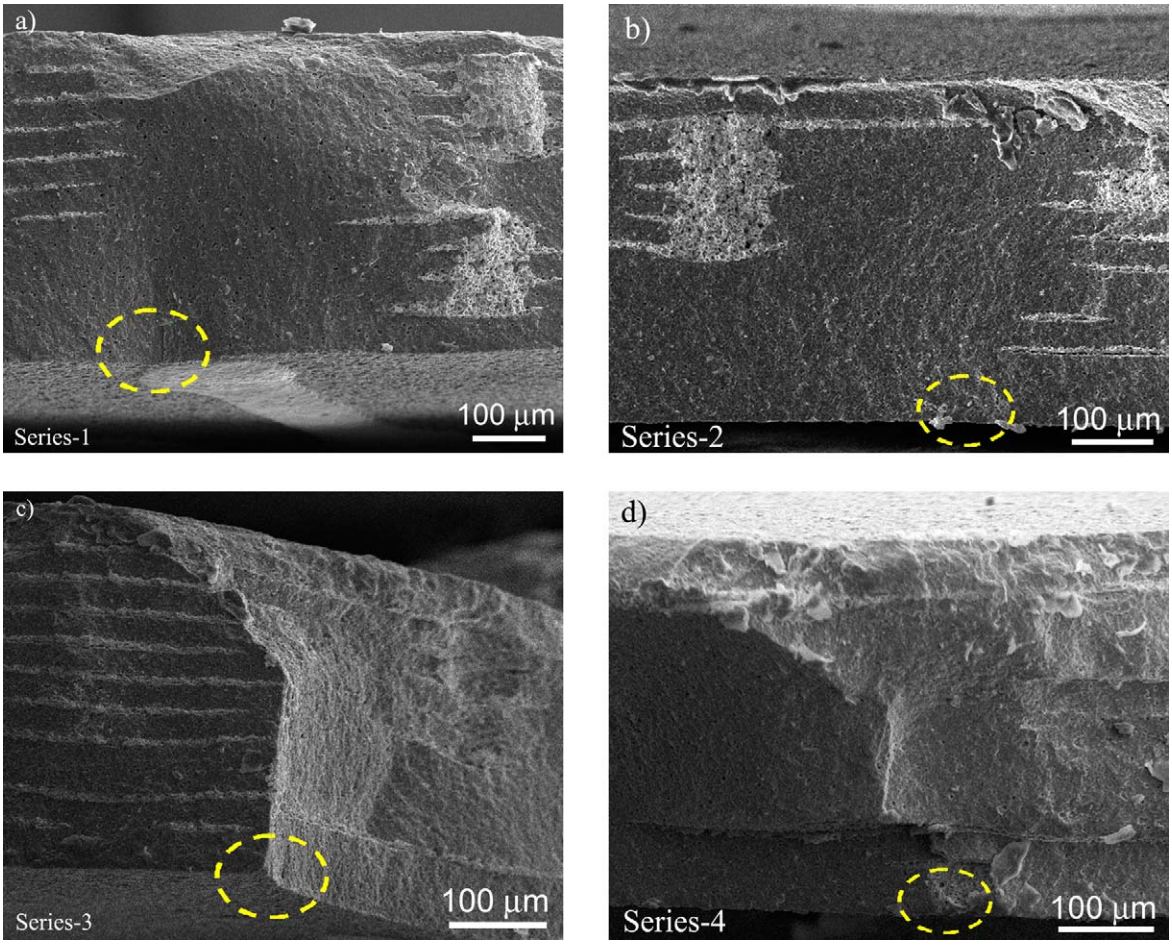

Fig. 7. SEM micrographs of the fracture surface of four specimens corresponding to series 1 (a)–4 (d) with the upper side tested under tension. The tensile surface is placed downwards.

Table 2
Estimated critical flaw size, a_c, corresponding to the maximum and minimum failure stress value respectively, for all series under both configurations as well as for the bulk specimens.

Series	Estimated critical flaw size range, a_c [μm]	
	Upper side under tension	Lower side under tension
Series 1	(20.4–5.7)	(16.8–7.5)
Series 2	(7.8–4.0)	(15.5–8.1)
Series 3	(12.2–5.7)	(12.8–5.9)
Series 4	(14.4–7.8)	(15.3–7.2)
Bulk	(4.3–9.4)	

where Y is a dimensionless geometric factor depending on the shape of the defect and loading configuration. Considering failure origins at the surface, it can be assumed $Y = 1.12$. The fracture toughness has been determined by means of the Single Edge V-Notch Beam (SEVNB) method[36] on standard flexural specimens (45 mm × 4 mm × 3 mm) tested under four-point bend,[37] resulting in $K_{Ic} = 1.8 \pm 0.1$ MPa m$^{1/2}$. According to Eq. (3) the estimated critical flaw sizes (corresponding to the maximum and minimum failure stress value of each sample), for all series under both configurations as well as for the bulk specimens, are given in Table 2. It can be inferred that the estimated critical defects range between 4 and 21 μm. We caution the reader that large flaws (*i.e.* ≈20 μm) could only be predicted (according to Eq. (3)) for series 1, which correspond to locations near vias. This opens the possibility that low strength values be associated with stress concentrations at such location and not with larger material flaws.

In order to explain the differences between series for the case of upper side under tension (Fig. 5) and the very similar strength distributions for the other case, *i.e.* lower side under tension (Fig. 6), a fractographic analysis was performed.

3.3. Fractographic analysis of broken specimens

The different load–displacement curves (see Fig. 4) recorded between bulk specimens and certain series (with metallisation) suggested the effect of the metal layers on the crack propagation through the LTCC. The examination of the fracture surfaces showed in fact a different crack path depending on the inner architecture under the tested region. An example corresponding to this fractographic analysis is shown in Fig. 7 (specimens with upper side under tension), where the influence of the internal metal layered structure in the crack path at fracture can be appreciated. While a straight crack pattern was found for bulk LTCCs as well as for LTCCs with mainly glass–ceramic content under the tested surface (such as in Fig. 7a and b), a step-wise fracture (load-steps events in the load–displacement curves from Fig. 4a) could be observed for LTCCs with metallic layers under-

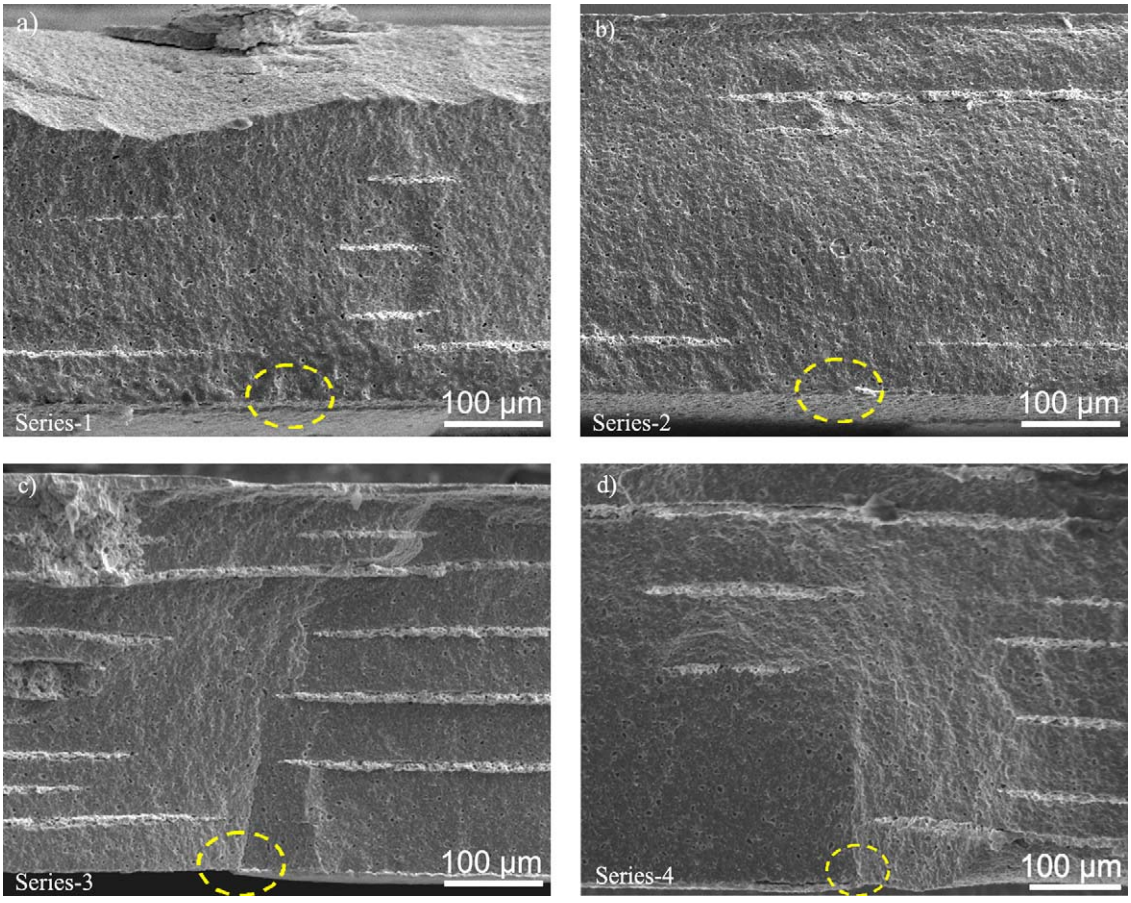

Fig. 8. SEM micrographs of the fracture surface of four specimens corresponding to series 1 (a)–4 (d) with the lower side tested under tension. The tensile surface is placed downwards.

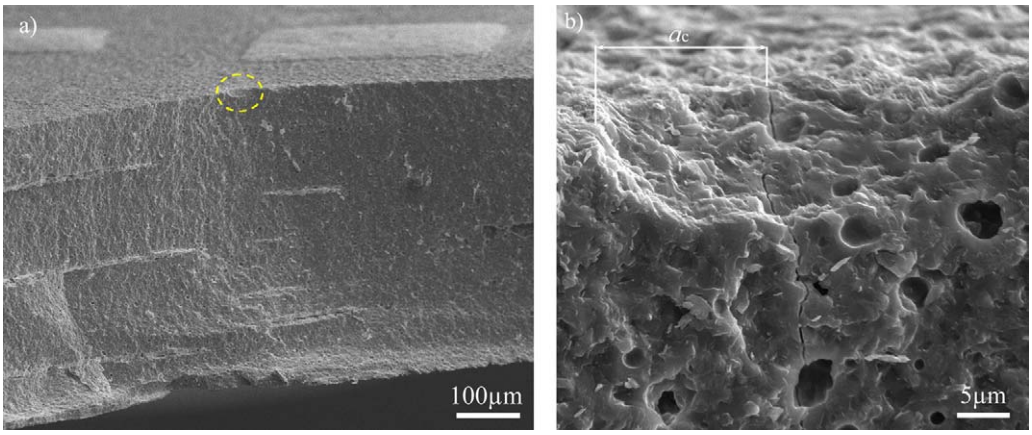

Fig. 9. a) SEM micrograph of the fracture surface of a specimen tested with the upper side under tension. b) Detail of a crack initiated at the centre of the origin and running normal to the main crack causing the failure during biaxial bending.

neath the surface (as shown in Fig. 7c and d). This might favour crack deflection mechanisms and thus avoid the catastrophic failure of the part. However, the rather far distance from the first metal layer (between 50 and 100 μm) to the surface of the specimen seems not to be very effective for crack arrest. Layer structures with near metal layers should be positioned at distances no farther than the size of critical defects found in the bulk material (*i.e.* around 20 μm). This will be further investigated by the authors and simple architectures with metal layers near the surface will be fabricated to search for an effective barrier to crack propagation.

Analogous to the previous case, for the specimens tested with the lower side under tension, most of the broken specimens showed step-wise fracture during the mechanical tests (as inferred from Fig. 4b). This can be associated with the fact that a metal layer is located (from design) underneath the lower side of the LTCC, covering almost the entire part. Hence, independent of the location tested with the B3Bs, the metal layer may act as a barrier to the initial crack propagation during fracture. This would explain the similar characteristic strength distribution of the four locations (see Fig. 6). Some SEM micrographs corresponding to fracture surfaces of specimens tested under this configuration are shown in Fig. 8. It can be appreciated that in all series a metal layer is located below the surface under tension. In this regard, particular attention should be paid to the shape of the Weibull plots in Fig. 5, for series 3 and 4. In such locations metal layers at a distance of approx. 50 μm from the surface are placed beneath the area of maximum stress during biaxial loading. This may explain the "*concave banana-shape*" in the Weibull diagram, which would be related to the fact that large cracks (initially propagating from the tensile surface) could be "arrested" (or deviated from straight path) by the first metal layer, thus yielding a minimum strength level for these components.

In an attempt to identify critical flaws initiating the fracture, a detailed analysis of broken specimens (both with the upper and lower side under tension) was performed. In all cases the source of failure could be found located at or near the surface of the LTCC (see for instance Fig. 9). In the cases where it was possible to discern the failure origin, the size of the flaws causing failure (as in Fig. 9) was in good agreement with the critical flaw size, a_c, predicted with Eq. (3). Natural flaws such as pores or agglomerates could however not be identified as fracture origins. Only in some cases could the fracture origin be found at the interface ceramic-vias (see Fig. 7a), most likely associated with stress concentrations, as also reported in literature for this type of architecture.[15] This could explain the relative large flaw sizes estimated with Eq. (3) for series 1 (*i.e.* ≈20 μm).

To sum up, the role of the metal layers on the strength and crack propagation in these materials should be further investigated, in order to design more reliable LTCC components, where metal layer structures may be tailored in the design to act as reinforcement mechanisms against brittle fracture. In this regard, simple structures are planned to assess the effect of the metal layer on the crack propagation. In addition, the effect of environmental conditions (temperature and humidity) as well as loading rate during testing should be taken into account to assess the mechanical reliability and life time of these complex structures.

4. Conclusions

The effect of metallisation on the mechanical response of commercial low temperature co-fired ceramics (LTCCs) was assessed using the ball-on-three-balls test, which allowed the evaluation of biaxial strength at specific locations in the component.

While the specimens tested with the lower side under tension resulted in a similar characteristic strength independent of the testing location, *i.e.* $\sigma_0 = 281–294$ MPa, the specimens tested with the upper side under tension at different positions showed a statistically significant difference in strength ($\sigma_0 = 283–383$ MPa). For locations of high ceramic content the strength of LTCCs with metal structures was similar to that of bulk material (*i.e.* $\sigma_0 = 370$ MPa).

Regarding the Weibull moduli, no statistical difference could be found between both orientations, resulting in $m = 8.9–12.4$ and $m = 9.3–15.3$ respectively, being also similar for bulk specimens ($m = 9.7$).

The examination of the fracture surfaces showed a different crack path depending on the inner architecture of the region of

maximum stress. It was found that when the LTCC is designed with a metal layer located underneath the tensile surface, initial cracks may be "deviated" from straight path, thus yielding a higher fracture resistance to the LTCC.

Acknowledgements

Financial support by the Austrian Federal Government (in particular from the Bundesministerium für Verkehr, Innovation und Technologie and the Bundesministerium für Wirtschaft und Arbeit) and the Styrian Provincial Government, represented by Österreichische Forschungsförderungsgesellschaft mbH and by Steirische Wirtschaftsförderungsgesellschaft mbH, within the research activities of the K2 Competence Centre on "Integrated Research in Materials, Processing and Product Engineering", operated by the Materials Centre Leoben Forschung GmbH in the framework of the Austrian COMET Competence Centre Programme, is gratefully acknowledged. The authors would also like to thank Mr. Franz Aldrian (EPCOS-OHG, Deutschlandsberg, Austria) for providing the specimens for this investigation.

References

1. Imanaka Y. *Multilayered low temperature cofired ceramics (LTCC) technology*. New York, NY 10013, USA: Springer Science-Business Media I; 2005.
2. Ewsuk KG. Ceramic-filled-glass composite sintering. *Ceram Trans* 1990;**15**:279–95.
3. Weibull W. *A statistical theory of strength of materials*. Royal Swedish Institute for Engineering Research; 1939. pp. 1–45.
4. Danzer R, Lube T, Supancic P. Monte-Carlo simulations of strength distributions of brittle materials—type of distribution, specimen and sample size. *Zeitschrift für Metallkunde* 2001;**92**:773–83.
5. Danzer R. Some notes on the correlation between fracture and defect statistics: are Weibull statistics valid for very small specimens? *J Eur Ceram Soc* 2006;**26**:3043–9.
6. Danzer R, Lube T, Supancic P, Damani R. Fracture of ceramics. *Adv Eng Mater* 2008;**10**:275–98.
7. Evans AG. Perspective on the development of high-toughness ceramics. *J Am Ceram Soc* 1990;**73**:187–206.
8. Clegg WJ, Kendall K, Alford NM, Button TW, Birchall JD. A simple way to make tough ceramics. *Nature* 1990;**347**:455–7.
9. Chan HM. Layered ceramics: processing and mechanical behavior. *Annu Rev Mater Sci* 1997;**27**:249–82.
10. Rao M, Sanchez-Herencia J, Beltz G, McMeeking RM, Lange F. Laminar ceramics that exhibit a threshold strength. *Science* 1999;**286**:102–5.
11. Lawn B. Ceramic-based layer structures for biomechanical applications. *Curr Opin Solid Stat Mater Sci* 2002;**6**:229–35.
12. Sglavo VM, Bertoldi M. Design and production of ceramic laminates with high mechanical resistance and reliability. *Acta Mater* 2006;**54**:4929–37.
13. Bermejo R, Pascual J, Lube T, Danzer R. Optimal strength and toughness of Al_2O_3–ZrO_2 laminates designed with external or internal compressive layers. *J Eur Ceram Soc* 2008;**28**:1575–83.
14. Mohanram A, Lee S-H, Messing GL, Green DJ. Constrained sintering of low-temperature co-fired ceramics. *J Am Ceram Soc* 2006;**89**:1923–9.
15. Dannheim H, Roosen A, Schmid U. Effect of metallization on the lifetime prediction of mechanically stressed low-temperature co-fired ceramics multilayers. *J Am Ceram Soc* 2005;**88**:2188–94.
16. Shetty DK, Rosenfield AR, McGuire P, Bansal GK, Duckworth WH. Biaxial flexure tests for ceramics. *Ceram Bull* 1980;**59**:1193–7.
17. Dannheim H, Schmid U, Roosen A. Lifetime prediction for mechanically stressed low temperature co-fired ceramics. *J Eur Ceram Soc* 2004;**24**:2187–92.
18. Tandon R, Newton CS, Monroe SL, Glass SJ, Roth CJ. *Sub-critical crack growth behavior of a low-temperature co-fired ceramic*, vol. 90; 2007. pp. 1527–1533.
19. Morrell R, McCormick N, Bevan J, Lodeiro M, Margetson J. Biaxial disc flexure—modulus and strength testing. *Brit Ceram Proc* 1999;**59**:31–44.
20. Börger A, Supancic P, Danzer R. The ball on three balls test for strength testing of brittle discs—stress distribution in the disc. *J Eur Ceram Soc* 2002;**22**:1425–36.
21. Börger A, Supancic P, Danzer R. The ball on three balls test for strength testing of brittle discs—Part II. Analysis of possible errors in the strength determination. *J Eur Ceram Soc* 2004;**24**:2917–28.
22. Danzer R, Supancic P, Harrer W. Biaxial tensile strength test for brittle rectangular plates. *J Ceram Soc Jpn* 2006;**114**:1054–60.
23. Danzer R, Harrer W, Supancic P, Lube T, Wang Z, Börger A. The ball on three balls test—strength and failure analysis of different materials. *J Eur Ceram Soc* 2007;**27**:1481–5.
24. Börger A, Supancic P, Danzer R. The ball on three balls test for strength testing of brittle discs: stress distribution in the disc. *J Eur Ceram Soc* 2002;**22**:1425–36.
25. *Guide to ANSYS user programmable features. ANSYS release 11.0*; 2007.
26. Lins W, Kaindl G, Peterlik H, Kromp K. A novel resonant beam technique to determine the elastic moduli in dependence on orientation and temperature up to 2000 °C. *Rev Sci Instrum* 1999;**70**:3052–8.
27. Bermejo R, Kraleva I, Antoni M, Supancic P, Morrell R. Influence of internal architectures on the fracture response of LTCC components. *Key Eng Mater* 2009;**409**:275–8.
28. Morrell R. *Fractography of brittle materials. Measurement good practice guide no. 14*. Teddington, UK: Laboratory NP; 1999.
29. Danzer R. Mechanical failure of advanced ceramics: the value of fractography. *Key Eng Mater* 2002;**223**:1–18.
30. ENV 843-5. *Advanced technical ceramics—monolithic ceramics—mechanical tests at room temperature—part 5: statistical analysis*; 1997.
31. Lugovy M, Slyunyayev V, Subbotin V, Orlovskaya N, Gogotsi G. Crack arrest in Si_3N_4-based layered composites with residual stress. *Comp Sci Technol* 2004;**64**:1947–57.
32. Sglavo VM, Paternoster M, Bertoldi M. Tailored residual stresses in high reliability alumina–mullite ceramic laminates. *J Am Ceram Soc* 2005;**88**:2826–32.
33. Bermejo R, Sánchez-Herencia AJ, Llanes L, Baudín C. High-temperature mechanical behaviour of flaw tolerant alumina–zirconia multilayered ceramics. *Acta Mater* 2007;**55**:4891–901.
34. Griffith AA. The phenomenon of rupture and flow in solids. *Phil Trans Roy Soc London* 1921;**A221**:163–98.
35. Danzer R, Lube T, Supancic P, Damani R. Fracture of advanced ceramics. *Adv Eng Mater* 2008;**10**:275–98.
36. Kübler J, Danzer R, Fett T, Damani R. *Notch width—theory and model: VAMAS report no. 37, ESIS document D2-99*; 1999.
37. EN-843-1. *Advanced technical ceramics, monolithic ceramics, mechanical properties at room temperature, part 1: determination of flexural strength*; 1995.